Desalination 566 (2023) 116899

Contents lists available at ScienceDirect

Desalination

journal homepage: www.elsevier.com/locate/desal

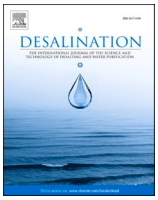

SofTer: Theory, software, and video tutorial for simulating capacitive deionization with tertiary current distributions

Johan Nordstrand

Functional & NanoMaterials Group, Applied Physics Department, School of Engineering Sciences, KTH Royal Institute of Technology, Hannes Alfvéns väg 12, 114 19 Stockholm, Sweden
Now at: Department of Chemistry, Stanford University, Stanford, California 94305, USA

HIGHLIGHTS

- Complexity and instability from rapid physical changes limit simulations of CDI
- A numerically stabilized model with a tertiary current distribution is introduced
- The model covers CDI, MCDI, FCDI, intercalation, multi-ion, and more
- Stability is benchmarked through computational speed
- Software and tutorial are presented

GRAPHICAL ABSTRACT

Type	Available
CDI (EDL)	✓
CDI (Intercalation)	✓
CDI (MCDI)	✓
CDI (FCDI)	✓
Multi-ion	✓
Flow by/through	✓
Flow cont./batch	✓
Charge CV or CC	✓
Pre-charge	✓
Auto switching	✓
Simulate 1D/2D	✓

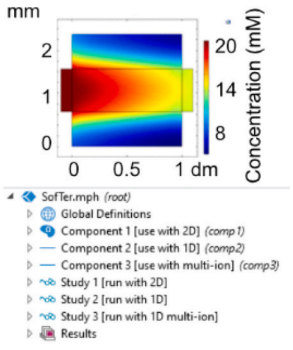

ARTICLE INFO

Keywords:
Capacitive deionization
Desalination
EDL
Finite element
Modeling
Tertiary

ABSTRACT

Capacitive deionization (CDI) is a desalination method that has been expanding substantially in recent years. As processes are getting more complex, corresponding developments in theory and software are necessary to keep up and drive future research. In this work, we derive a new CDI theory based on a tertiary current distribution, meaning each ionic species is resolved individually in a unified framework in 1D/2D. The results show that this approach is ideal for simulations with multiple ionic species and materials that affect cations and anions differently. Direct examples include such as intercalation materials and membranes. It is also effective for incorporating electrode replenishment in flow-electrode CDI (FCDI). By benchmarking with traditional methods, we demonstrate that numerical stability is a central limitation of traditional methods for these applications. The results identify physical processes involving rapid changes to cause major instabilities. This can thus be handled by introducing specific numerically stabilizing factors. Finally, the theory is compiled into comprehensive software that researchers can straightforwardly apply in future studies without having to reconstruct methods from scratch. A corresponding video tutorial has also been deposited. In conclusion, the work pushes the limits of the simulation capabilities in a wide range of CDI processes.

E-mail address: johanno3@kth.se.

https://doi.org/10.1016/j.desal.2023.116899
Received 11 May 2023; Received in revised form 15 July 2023; Accepted 2 August 2023
Available online 3 August 2023

1. Introduction

Capacitive deionization (CDI) is an emerging technology for purifying water [1–4]. The method is based on using a device with porous electrodes that store ions upon the application of a voltage. More than that, the research field has been growing rapidly in recent times. Meanwhile, researchers are increasingly looking towards complicated processes such as selective ion removal [5–7] and upscaled devices for pilot plants [8]. The scope of this technology is thus expanding at the same time as the processes are getting more complex. The complex mechanisms involved in the process make simulations essential for better understanding and developing the technology.

A variety of CDI processes exist that are relevant for simulations to cover. These can include a variety of operational [9], material [10,11], and structural conditions [12,13]. For instance, charging with constant voltage (CV) or constant current (CC) affects the charging dynamics and energy consumption. Flow between (fb-CDI) and flow through (ft-CDI) variants affect the pumping energy and the transport rate for the desalinated water [14]. Membrane CDI (MCDI) can raise charge efficiency at the cost of adding extra materials. Pre-charge treatments can also raise charge efficiency by changing the electrode surface structure [15]. Intercalation materials have high storage capacity, can be less sensitive to concentration levels in the solution, and have the potential to be ion-selective [16,17]. Flow electrode (FCDI) can be effective since the electrode mass is replenished continuously [12,18], as opposed to having a discharge phase. Multi-ion solutions will be relevant for any application with realistic water composition [19]. All these are covered in this work.

A fundamental challenge with these advanced methods from the simulation perspective is the complexity. For instance, intercalation materials or multi-ion solutions have a more complex theory than standard electrodes based on electric double layers (EDL). More than that, applications often call for a combination of methods. For instance, one might want to simulate ion selectivity in multi-ion solutions with intercalation materials. The increasing scope and complexity of these processes make simulation models increasingly difficult to construct and implement from scratch. Thus, corresponding developments in numerical methods and software are necessary to enable future theoretical studies in these areas.

In this work, we derive a comprehensive theory based on tertiary current distributions (TCD) that can include all these aspects under the same theoretical framework. The difference between TCD and previous modeling methods (e.g. [20,21]) is that all ionic species are simulated separately in a generalized framework. This is essential for predicting performance in multi-ion solutions, including selectivity. It is also important to materials that affect cations and anions differently, such as membranes and intercalation materials. This way of separating model components also leads to a natural way to describe electrode replenishment in FCDI. Overall, the method can be more precise and flexible since it is directly based on ionic and material properties. However, the challenge with this approach is numerical stability. Therefore, that will be a core focus of this work. As part of introducing the theory, we also explore the connections between different types of physical processes in CDI and their corresponding numerical stability with different numerical implementations. For instance, previous studies have found that ionic starvation leads to poor numerical performance.

Finally, we present SofTer: a new Software for Tertiary-current-distribution simulations of CDI, designed to soften the transition of research into increasingly broad and complex CDI processes. The idea is to make a wide range of CDI simulations more accessible to researchers while enabling new types of computational studies. One issue that the software solves is that model construction from scratch requires deep knowledge of numerical stabilization methods, or else the complex simulations can be too unstable [21,22]. Another strong point of significance for the software is its flexibility. The interfaces are pre-built and new devices can straightforwardly be tested by changing the model parameters or specific parts of the model. Put together, this study thus provides a deeper understanding of the physical and numerical aspects of CDI processes, and the software can enable a wide range of new studies.

2. Material and methods

These sections will present the theory and theoretical methods that underline the software.

2.1. Basic model

Here, we show how to construct a CDI model based on a tertiary current distribution.

2.1.1. Transport

The fundamental idea behind the CDI devices is to remove salt ions from a water stream. This means ions are moving, and the movement J_i for an ionic species i depends on diffusion, convection, and migration (Eq. (1)). Here, D_i is the diffusion constant, c_i is the concentration the solution, z_i is the valency, $u_{m,i}$ is the mobility, F is the Faraday constant, and ϕ_l is the local potential in the solution (l for liquid). A point to note is that the diffusion coefficient is the effective diffusion coefficient in the pores. It can be calculated from the real diffusion coefficient using the Bruggeman correction $D_i = D_{0,i}p_M^{3/2}$ ($D_{0,i}$ is the ideal diffusion coefficient and p_M is the macro-porosity). The ionic flux originates from adsorption $-R_i$ at the electrode surface (Eq. (2)). We will explain further how to calculate the adsorption rate in the next section, but this is how it connects with transport.

$$J_i = -D_i\nabla c_i - c_i u - z_i u_{m,i} F c_i \nabla\phi_l \tag{1}$$

$$\nabla\cdot J_i = R_i \tag{2}$$

The net transport of ions also means that a current is flowing through the device. The total local current in the solution i_l depends on the total ionic flux (Eq. (3), Σ_k denotes a sum over the ionic species). Meanwhile, there is a current i_s in the electrode matrix that depends on the electrode conductivity σ_s and the local electrode potential ϕ_s (Eq. (4)). Both currents originate from the adsorption rate (Eq. (5)).

$$i_l = F\Sigma_k z_k J_k \tag{3}$$

$$i_s = -\sigma_s\nabla\phi_s \tag{4}$$

$$\nabla\cdot i_l = -\nabla\cdot i_s = F\Sigma_k z_k R_k \tag{5}$$

2.1.2. Adsorption

The last section explained how an adsorption rate can generate a current and ionic flux in the device. Here, we elaborate on the adsorption part. In typical CDI materials, ions accumulate in EDLs in the pores on the electrode surface. According to the modified Donnan (mD) model of adsorption [21], a normal capacitor equation can be used to relate the charge storage q and the potential drop $\Delta\phi_m$ inside the micropores (Eq. (6)). There is also a potential drop $\Delta\phi_D$ required to maintain a concentration difference between the micropore c_m and the surrounding macropore (c_i, same as before). Here, $\overline{\mu}_{att}$ is a baseline micropore attraction (Eq. (7)).

The mD expression is the same as in Ref. [21], but we will implement it differently for convenience. The micropore concentration as originally described is in units of mol per micropore volume. That is, $c^*_{m,i} = p_m c_{m,i}$, with p_m being the micro-porosity and $c^*_{m,i}$ being the concentration in units of mol per electrode volume. By multiplying Eq. (7) with p_m, the equation can be expressed per electrode volume instead. We can here introduce the parameter $exp(\overline{\mu}^*_{att}) = p_m exp(\overline{\mu}_{att})$, so the equation looks the same except for the added *. A benefit of doing this is that we can

treat p_m and $exp(\bar{\mu}_{att})$ as a single fitting parameter instead of two.

$$\Delta\phi_m = \frac{q}{C_{dl}} \tag{6}$$

$$c_{m,i} = c_i exp(\bar{\mu}_{att}) exp(-z_i \Delta\phi_D / V_T) \tag{7}$$

The equilibrium-state potential drop E across the electrode is equal to the sum of these (Eq. (8)). The potential drop at any point in time can also be written as $(\phi_s - \phi_l)$. Hence, the overpotential follows Eq. (9) and describes the difference between the real potential drop and the equilibrium-state drop. For the EDL materials, the is no significant activation energy required so we typically assume the equilibrium state is reached at all times. This means the adsorption rate as described earlier is equal to whatever makes the overpotential zero.

$$E = \Delta\phi_m + \Delta\phi_D \tag{8}$$

$$\eta = (\phi_s - \phi_l) - E \tag{9}$$

2.1.3. External conditions

The last section showed how a potential drop across the electrode is required to get adsorption. The desalination thus starts when an external potential is applied to the device (Eq. (10)). Here, V is the voltage on the current collectors, V_{ext} is the external potential that is supplied to the device, R_c represent the resistive elements in the circuit, and I is the total current. In CV charging, the external voltage is constant. In CC, the current is constant instead. If the conductivity on the electrode matrix is very high, the local potential ϕ_e in the electrodes will be the same as the voltage V on the current collectors. However, to keep it generic, we have chosen to make the voltage V a boundary condition for the electrode potential.

$$V = V_{ext} - R_c I \tag{10}$$

Another input from the external environment is the influx of new water. In 2D, we require that concentration at the inlet maintains the inlet level c_{in}. Meanwhile, the outlet is represented by zero-gradient conditions (since the concentration is constant after exiting the device). In 1D, the influx of water instead becomes an ion source R_i, just as the electrode adsorption is a sink (Eq. (11)). Here, f is the volumetric flowrate and ν_{sp} is the spacer volume.

$$R_i = \frac{f}{\nu_{sp}} (c_{in,i} - c_i) \tag{11}$$

2.2. Numerical stabilization

In this work, we introduce several new methods for numerical stabilization. Stabilizations are important for enabling FEM computations at complex conditions and for improving the simulation speed.

2.2.1. Charging

We take some special theory approaches to make the calculations more numerically stable. The first one concerns the charging. As mentioned earlier, the traditional EDL models assume zero overpotential when calculating the adsorption rate. However, materials that do have a non-zero overpotential can typically be described with the Butler-Volmer (BV) equations [23] (Eq. (12), $i_{loc,i}$ is the local current). Here, the parameters are $i_{0,i}$ for the reference current, $\alpha_{c,i}$ for the cathodic transport coefficient, $\alpha_{a,i}$ for the anodic transfer coefficient, and η_i for the overpotential of each ionic species. This localized surface current translates to a volumetric current $i_{v,i} = a_v i_{loc,i}$ via the active specific surface area a_v.

$$i_{loc,i} = i_{0,i} \left(exp\left(\frac{\alpha_{a,i}\eta_i}{V_T}\right) - exp\left(\frac{-\alpha_{c,i}\eta_i}{V_T}\right) \right) \tag{12}$$

For small overpotentials, the expression above can be linearized and compressed (Eq. (13)). This makes it possible to express the current based on the overpotential and a resistance $R_{s,i}$. In the limit of low resistance, we get back to the classical approach that the EDL materials have zero overpotential. However, an interesting point here is that $R_{s,i}$ fulfills the role of a K-controller in the analogy of a control system. That is, even if the equilibrium state is supposed to hold exactly, we can allow for some devotion in the model and use $R_{s,i}$ as a controller to obtain the correct state. If $R_{s,i}$ is chosen to be small enough, the deviation becomes so small that the output result is the same as in the ideal case. But, the model is more numerically stable since the charge-storage conditions need not be exact at all times.

$$i_{v,i} = \eta / R_{s,i} \tag{13}$$

2.2.2. Adsorption balance

Another complication is the contribution of each ionic species to the total current. In a multi-ion solution, many combinations of adsorption lead to the same overall charge storage. Even in a single-ion solution, the balance between counterion adsorption and co-ion expulsion determines the charge efficiency. So, the question is how to stably generate the correct adsorption of each ionic species. The mD model shows what the concentration is supposed to be for each ion [21], so we will solve this with a control-theory approach too. The first step in solving the situation for the double-layer material is to consider that the current can affect only the first ionic species ($i_{v,i} = 0$ for $i > 1$). That is, we only set up the BV equations for the first species, leading to an ideal adsorption rate for that species (Eq. (14)). This step ensures that the total charge passed is correct. Aside from the aforementioned effect that the adsorption rate has on the solution concentration, it also determines the adsorption concentration c_m. So, $dc^*_{m,1}/dt = -R_1$.

$$R_1 = -\frac{i_v}{z_1 F} \tag{14}$$

The second step is to use the control approach to balance the adsorption of each species. At any time, the deviation e_i between the real adsorption $c^*_{m,i}$ and the adsorption we would have with the correct balance given by Eq. (15). This error can then be corrected using a proportional controller k_b (Eq. (16)). As before, $dc_{m,i}/dt = -R_i$ for each species, and $c^*_{m,i}$ is tracked for all species. Notably, the first ionic species will have contributions to R from both the charging above and the balancing here, and these effects stack.

$$e_i = -\left(c^*_{m,i} - c_i exp(\bar{\mu}^*_{att}) exp(-z_i \Delta\phi_D / V_T) \right) \tag{15}$$

$$R_i = -k_b e_i \tag{16}$$

The tricky part here is how to define the $\Delta\phi_m$ and $\Delta\phi_D$ potentials when we relax the conditions for adsorption balance. However, balancing the adsorption is not supposed to change the total charge storage, so we should still have $d\Delta\phi_m/dt = dq/dt/C_{dl} = i_v/C_{dl}$. Meanwhile, $\Delta\phi_D$ is defined as the potential that gives the correct average balance (Eq. (17), and the colon ":" in the equation indicates that the variable is implicitly defined and calculated with a nonlinear solver at each time step). Notably, the sum in the equation changes strictly with the potential, meaning it must have a unique solution.

$$\Delta\phi_D : \Sigma_i z_i e_i = 0 \tag{17}$$

Using this definition of the Donnan potential, we can now verify that the balancing reactions do not affect the total charge storage on the electrodes. In Eq. (18), the expression on the left shows the change in charge from all the R values, and the last equality follows from the definition of $\Delta\phi_D$.

$$\Sigma_i z_i R_i = -k_b \Sigma_i z_i e_i = 0 \tag{18}$$

Put together, we have thus separated the charge and adsorption into two parts that are solved separately. The first calculates the charge based on the BV equation and attributes all charge to the first ionic species. The

second balances the adsorption of all ionic species to keep the balance in Eq. (7) without changing the total charging state.

2.2.3. Concentration shocks

A classic problem with FEM simulations of CDI is that the computations become highly unstable when the concentration becomes too low. Typically, the problem originates in that the concentration becomes depleted in the electrode but high in the channel, so there is a sharp gradient between these regions.

One way to address this is to introduce an artificial potential that becomes active when the concentration is too low. So, the previous equilibrium potential is replaced with an effective potential $E_{eff} = E + E_{stab}$, wherein $E_{stab} = V_{stab}\text{step}(c/c_{init})$. Here, c is the concentration of the ionic species being adsorbed at each electrode and c_{init} is the initial potential. The step function is a smooth function that goes from 0 to 1 when c/c_{init} becomes too low (as defined in COMSOL). Specifically, it decreases over an interval $\Delta\bar{c}_{stab}$ centered at $\bar{c}_{stab,0}$. The values of these stabilization parameters are not critical, although they should be chosen to be small enough to not significantly change the simulation results while also performing the stabilization. The fundamental idea is just that they prevent the concentration from reaching too close to zero. We chose $\bar{c}_{stab,0} = 0.025$ and $\Delta\bar{c}_{stab} = 2\bar{c}_{stab,0}$. This means the stabilization starts to have an effect when the concentration in the pores drops below 5 % of the initial concentration. We have chosen the stabilization voltage V_{stab} to be equal in magnitude to the external/maximum voltage. It is positive in the anode and negative in the cathode. The magnitude is chosen to be just as big as it needs to be to guarantee that no more adsorption can happen when the step function is fully activated.

2.2.4. Fundamental methods

Some basic stabilization methods from earlier works are also employed. For instance, the simulation starts in equilibrium, and parameters such as the external voltage (in CV) or current (In CC) are smoothly raised from zero over a short time, instead of directly jumping to the correct value. This approach makes the computation more stable since change happens gradually. Also, events are employed in the FEM implementation, meaning the simulation is reinitialized at the switching points. This makes the simulation more stable when the switching causes a rapid change in the system parameters. Another point to note is that meshing is chosen to be denser in the more sensitive regions, especially the interfaces between the electrodes and the spacer.

2.3. Basic parameter fitting

Two fundamental fitting parameters relate to the circuit behavior of the CDI device. The first parameter is the circuit resistance, which can be calculated from a fitting experiment from the current/voltage response. In a fitting experiment with CV charging, we have $R_c = V_{CV}/I_P$, for a CV voltage V_{CV} and a measured peak current of I_P. In a fitting experiment with CC charging, we have $R_c = V_0/I_{CC}$, for a current I_{CC} and a measured starting voltage V_0 after the current is applied. The second parameter is the total capacitance C_{dl}. This can be calculated as $C_{dl} = Q/V$ as normal for a capacitor, with V being the voltage (resistive losses to included) that is required to store a charge Q.

A third parameter is the micropore attraction (single-ion solution), which determines the charge efficiency. See also the section about pre-charged electrodes. In a multi-ion solution, every extra ionic species introduces one more attraction parameter. The simplest way of fitting the attraction parameters is to calculate the circuit fitting parameters first and then just test a few values of the attraction parameter. Higher values always reduce the charge efficiency, so it is straightforward to figure out how to change it to get a good value. In a multi-ion solution, higher micropore attraction values can also raise the relative adsorption of one ionic species compared to the rest.

A less arbitrary method of calculating the micropore attraction for a single-ion solution is shown in Eq. (19). If the fitting voltage is reasonably high (>0.4 V, approximately), then most of the co-ions will have been expelled. This means the micropore attraction can be calculated from the charge efficiency Λ and the fraction of initial co-ion loading to the total removal Γ (unit mol) (Eq. (20)). Here, c_{init} is the initial concentration and ν_{el} is the electrode volume. In a single-ion solution, the same attraction parameter can be used for both the anion and the cation. An even more thorough derivation can be found in Ref. [21].

$$\frac{c_{init}exp\left(\bar{\mu}^*_{att}\right)\nu_{el}}{\Gamma} = 1 - \Lambda \tag{19}$$

$$exp\left(\bar{\mu}^*_{att}\right) = \frac{1}{c_{init}\nu_{el}}\Gamma(1-\Lambda) \tag{20}$$

In the multi-ion case, more information is needed to separate the contributions from each ionic species. Specifically, the parameter values can be determined if the net adsorption Γ_i is measured for each ionic species. In that case, we can get the total adsorption by summing the micropore concentrations of all ionic species for both electrodes and subtracting the corresponding initial values (initial means $\Delta\phi_D = 0$). That leads to Eq. (21). The formulation here assumes a continuous mode, such that the initial and equilibrium macropore concentration are the same. However, corresponding equations can be derived for the batch mode, if necessary. An extra piece of information is also required to determine $\Delta\phi_D$, which can be obtained by looking at the total charge storage (Eq. (22)). In this case, Eqs. (21) and (22) should be solved jointly for all ionic species to get an estimate of $exp\left(\bar{\mu}^*_{att,i}\right)$ for all i together with one $\Delta\phi_D$. So, there are N + 1 equations in total for N ionic species, and a non-linear numerical solver is required to extract the parameter values. The units are mol for Γ_i and C for Q.

$$\Gamma_i = 2\nu_{el}c_{init,i}exp\left(\bar{\mu}^*_{att,i}\right)(cosh(-z_i\Delta\phi_D/V_T) - 1) \tag{21}$$

$$Q = \Sigma_i 2z_i\nu_{el}c_{init,i}exp\left(\bar{\mu}^*_{att,i}\right)sinh(-z_i\Delta\phi_D/V_T) \tag{22}$$

2.4. Advanced model

2.4.1. MCDI

Membranes are described here as internal boundary conditions. That is, we are neglecting the thickness of the membrane, for simplicity. Also, it is assumed that the membrane is fully blocking the ionic species that are supposed to be blocked. A membrane with special resolution could also be introduced, but having these assumptions makes the software more tractable.

Based on the assumptions, the membrane is fully blocking all ions except for some species c_i which has concentration $c_{i,u}$ on one side of the membrane and the concentration $c_{i,d}$ on the other (Eq. (23)). This leads to an equilibrium potential drop $\Delta\phi_{mem}$ across the membrane. If the potential drop is higher than the equilibrium value, there will be a current i_{mem} across the membrane (Eq. (24)). The magnitude of this current depends on the electrolyte conductivity in the membrane σ_{mem} and the membrane thickness d_{mem}. Notably, most of the resistance can be attributed to the circuit resistance R_c in typical simulations. This means the exact values of the conductivity and thickness will not have a significant impact. The main effect of enabling membranes in the software is that some ions are blocked completely, which is the major function of the membranes.

$$\Delta\phi_{mem} = -\frac{RT}{z_iF}ln\left(\frac{c_{i,u}}{c_{i,d}}\right) \tag{23}$$

$$i_{mem} = -\frac{\sigma_{mem}}{d_{mem}}\left(\phi_{l,u} - \phi_{l,u} - \Delta\phi_{mem}\right) \tag{24}$$

The main benefit of this approach with thin membranes on internal boundaries is that the geometry stays the same irrespective of whether a membrane is present or not. All that is required to switch between CDI and MCDI is thus to enable/disable the membrane interface. That is practical since the same model can be used for both CDI and MCDI.

2.4.2. Batch flow

As written earlier, the inflow concentration c_{in} affects how the CDI device is replenished with new ions. In the case of a continuous flow mode, the inlet concentration is constant. However, it will change if a batch mode is used. In Eq. (25), f is the volumetric flowrate, ν_{batch} is the batch volume, and c_{out} is the effluent concentration. In 2D, the effluent concentration is measured in the outlet pipe (the end of the spacer region). In 1D, the effluent concentration is the average concentration in the spacer (assuming fb-CDI, otherwise the effluent concentration is measured at the outlet end).

$$\frac{dc_{in}}{dt} = \frac{f}{\nu_{batch}}(c_{out} - c_{in}) \tag{25}$$

2.4.3. Electrode pre-charge

Some electrode treatments change the baseline potential of the electrodes. This is straightforward to apply here since the charge is already described in terms of the electrode potential E. By adding pre-charge, we can replace E with an effective potential $E_{eff} = E + E_{pre}$. So, E_{pre} is the induced potential shift from the electrode treatment. Notably, it changes the point-of-zero-charge (PZC).

A point to note here is the connection between the pre-charging and the micropore attraction. If the PZC is at 0 V, that means the micropores are net uncharged when the voltage is zero. From the earlier Eq. (9), we can see that this means the Donnan potential is also zero. So, the conditions of this PZC are written in Eq. (26) (N is the number of ionic species). Using this, one attraction parameter can be calculated based on the other ones (Eq. (27)). This can also be written as the projection of the vector of exponential micropore attractions on the 1-norm normalized vector of charges in the solution (Eq. (28), charge neutrality gives the new expression in the denominator). In a solution with a single anion and a single cation, this means the micropore attractions are identical (so only one needs to be fitted, as in Ref. [21]). If the PZC is not zero, the idea is to calculate the micropore attractions as if it was zero anyway and then add the pre-charge via E_{pre}, thus separating the effects. That is, E_{pre} represents the net charge while the micropore attraction represent the charge-neutral pre-loading of both anions and cations.

$$PZC = 0 \rightarrow 0 = \Sigma_{k=1:N} z_k c_k exp\left(\overline{\mu}^*_{att,k}\right) \tag{26}$$

$$exp\left(\overline{\mu}^*_{att,N}\right) = -\frac{\Sigma_{k=1:N-1} z_k c_k exp\left(\overline{\mu}^*_{att,k}\right)}{z_N c_N} \tag{27}$$

$$exp\left(\overline{\mu}^*_{att,N}\right) = \frac{\Sigma_{k=1:N-1} z_k c_k exp\left(\overline{\mu}^*_{att,k}\right)}{\Sigma_{k=1:N-1} z_k c_k} \tag{28}$$

The method presented above is one way of simplifying the fitting process by eliminating one attraction parameter. However, it is also possible to ignore E_{pre} and just fit all attraction parameters independently. Still, the value of the suggested approach is that if E_{pre} can be measured separately (or reasonably presumed to be zero), then there are fewer parameters to fit, meaning the fitting process is more stable.

Another point to note is that concentration in the solution will affect the PZC, as can be seen in the equations (for instance, changing the concentrations in Eq. (27) affects how much each micropore attraction parameter influences the final attraction parameter). So, the micropore attractions are supposed to be calculated for the set of concentrations in the fitting experiment, and then we just note that varying concentrations will give some shifts that are independent of both the pre-charging and the micropore attraction.

2.4.4. Intercalation materials

In the section about double-layer materials, we described how to calculate the charging and adsorption based on the equilibrium potential E. For intercalation materials, the model framework is similar but the potential E is given by the extended Frumkin equation (Eq. (29)) [5,16,24]. Here, $E_{i,ref}$ is a constant reference potential for the given intercalation, $c_{\mathrm{ref}} = 1\,M$ is a reference concentration, g_i is a constant interaction parameter, and c_i is the concentration in the electrode pores. Also, $\theta_i = c_{s,i}/c_{s,i,max}$ and describes the fraction of adsorbed concentration on the particle surface $c_{s,i}$ to the maximum concentration (subscript s for solid phase in the particles). That is, θ_i represents the state of charge (soc).

$$E = E_{i,ref} - V_T\left(ln\left(\frac{\theta_i}{1-\theta_i}\right) - ln\left(\frac{c_i}{c_{ref}}\right)\right) - g_i(\theta_i - 1/2) \tag{29}$$

The logarithmic terms have almost no effect on the potential unless the is close to 0 or 1, or if the concentration is nearly 0. However, the potential magnitude increases infinitely as these limits are approached, meaning the limits will never be passed. The term with g_i instead describes interaction energy in the adsorbed concentration. We could say that the free energy from ion-ion interaction should follow $f \propto g_1\theta_i^2$, and the chemical potential is $\mu_i \propto \partial f/\partial\theta_i$, hence the linear form in the equation.

If there are more than one ionic species, each species will have a separate potential E_i of the form in Eq. (30). Here, $g_{avg} = \left(g_i + g_j\right)\Big/2$ is the average interaction energy, based on taking the free energy in the ionic mixture as $f \propto g_i\theta_i^2 + g_j\theta_j^2 + 2g_{avg}\theta_i\theta_j$.

$$E_i = E_{i,ref} - V_T\left(ln\left(\frac{\theta_i}{1-\theta_i-\theta_j}\right) - ln\left(\frac{c_i}{c_{ref}}\right)\right) - g_i(\theta_i - 1/2) - g_{avg}\theta_j \tag{30}$$

As before, the local current will depend on the overpotential. However, now the resistance is a real resistance and not just a stabilization factor.

A central difference with the intercalation materials is that the intercalation particles have a depth. So, the equations with E describe the relationship between the potential and the concentration at the particle surface. In addition, the ions can diffuse deeper into the particles, as described by Fick's law (Eq. (31), x_p is the particle spatial coordinate and $D_{s,i}$ is the diffusion constant in the particles). Consequently, the boundary conditions for the particles are as in Eq. (32). Notably, we have chosen 1D particles here, but they could just as well be spherical or something else. The unit of the concentration $c_{s,i}$ is moles per particle depth per electrode volume. That is, the particle surface-to-volume ratio and the particle density are implicit in $c_{s,max}$, the maximum concentration in the particles per electrode volume. If the total storage capacity is $\Gamma\,[mol]$ for an electrode with volume ν_{el} and particle depth L_s, the maximal concentration would be $c_{s,max} = \Gamma/\nu_{\mathrm{el}}/L_s$.

$$\frac{\partial c_{s,i}}{\partial t} = -D_{s,i}\frac{\partial^2 c_{s,i}}{\partial {x_p}^2} \tag{31}$$

$$\frac{\partial c_{s,i}}{\partial t} = -D_{s,i}\frac{\partial^2 c_{s,i}}{\partial {x_p}^2} - R_i \tag{32}$$

2.4.5. FCDI

The idea in the FCDI simulations is to treat the influx of new carbon particles (electrode) in the same way as the influx of ions (spacer). An influx of new carbon means that the adsorbed concentration is replaced (Eq. (33)), so the change in adsorption depends on the difference in the adsorption now $c_{ads,i}$ and the adsorption of the entering particles $c_{0,ads,i} = c_{init,i}exp\left(\overline{\mu}^*_{att}\right)$. We should also note that the influx changes the total charge storage on the particles, which is measured via the micropore

potential $\Delta\phi_m$ (Eq. (34)). In the equations, f_{el} is the electrode flowrate and ν_{el} is the electrode volume.

$$\frac{dc_{ads,i}}{dt} = -R_i\frac{f_{el}}{\nu_{el}}\left(c_{ads,i} - c_{0,ads,i}\right) \tag{33}$$

$$\frac{d\Delta\phi_m}{dt} = \frac{1}{C_{dl}}\frac{dq}{dt} = \frac{i_v}{C_{dl}} + \frac{F}{C_{dl}}\Sigma_i\frac{f_{el}}{\nu_{el}}\left(c_{ads,i} - c_{0,ads,i}\right) \tag{34}$$

One thing that makes this formulation tractable is that the model reverts to the basic model if $f_{el} = 0$. Thus, the same model can be used for both CDI and FCDI. That is promising for constructing a unified software of CDI.

The above formulation is the correct description in 1D. In 2D, it neglects the variation along the length of the flow pathway for the electrode particles. So, it is an approximation but does not contain all the information. A more appropriate method in 2D would be to track the adsorbed concentrations in the same way as the free concentration, with inlet/outlet conditions and flow coupling. The issue with this method, in our experience, is that it introduces substantial numerical instability. Putting entry pipes for the electrodes alleviates some of the problems at the boundary, but the simulations are still cumbersome. Because we wanted to focus on laptop-scale simulations, these features were excluded from the software. However, we will share them upon reasonable request.

2.5. Advanced numerical stabilization

2.5.1. Intercalation

The logarithmic terms in the Frumkin isotherm work fine in theory because they prevent the state of charge from going above 100 % or below 0 %. The problem in the practical case is that a large change in soc. is required to make a noticeable change in the logarithm. This can lead to "division by zero" errors in the numerical solver. It usually happens in CV modes wherein the charging is suddenly suppressed when the soc. reaches close to 100 %. It can also happen in CC modes when the soc. limit for switching is close to 0 or 100 %. To address this, we replace the Frumkin potential E with an effective potential $E_{eff} = E + E_{stab}$. The stabilizing voltage is defined in Eq. (35). The step function (as defined in COMSOL) goes from 0 to 1 as the argument becomes too low. Specifically, the change happens over an argument interval $\Delta\theta$ centered at θ_0. We chose $\theta_0 = 0.001$ and $\Delta\theta = 2\theta_0$. So, the practical impact on the simulation output is minuscule since the stabilization has no effect for soc. values that are farther away from 0 % or 100 % than this value of 0.001. The stabilization also depends on the constant stabilization potential, which we chose to be equal to the external/maximum potential. The point is just that it is supposed to be large enough that the intercalation stops when the step is activated.

$$E_{stab} = V_{stab}(step(\theta) - step(1-\theta)) \tag{35}$$

2.6. Advanced fitting

The advanced features contain more parameters than the basic model, but these are not fitting parameters. The maximum concentration in intercalation can be calculated as $c_{s,max} = \Gamma/\nu_{el}/L_s$, or more specifically $c_{s,max,i} = \Sigma/(z_i F \nu_{el} L_s)$, where is the maximum charge-storage capacity on the electrode and we note that the maximum concentration of different ionic species will depend on their valency. There are also parameters such as the diffusion constants $D_{s,i}$ that should be determined experimentally, as usual.

3. Experimental

The article is about theory and software, so this section will present the "computational experimental" aspects. That is, we will introduce how the case studies and tests were performed. Also, the software we used will be described to allow others to repeat and extend the benchmarking tests presented here.

3.1. Experiment data

To validate the theory, we have compared our simulation output with experimental data from reports in the literature. So, no new experiments were performed for this study. Rather, the studies were chosen so that the main new theory features could be evaluated relative to the results that previous simulation studies got with their experiment data. The data was extracted from graphs using the WebPlotDigitizer software. [25]

The figure caption corresponding to each case study contains a reference to the study from where the data originated. The data is presented in the same form as in the original works, so no additional processing has been performed. Rather, the simulations have been adapted to reflect the conditions in the experiment. The software has probes for voltage, current, concentration, cumulative current and concentration, etc. This means the simulation data in the result section could be outputted directly from the software. The one exception to this is the intercalation result, wherein the simulated voltage was converted to V vs. Ag/AgCl in the same way as described in the article from which the experiment data was extracted.

3.2. Software description

Software is presented along with this article. The software simulates time-dependent CDI processes and contains the theory presented in the theory section. The output includes currents and adsorption during the desalination and regeneration phases. The internal state of all concentrations, potentials, etc. can be viewed inside the device at any time step of the simulation. The user can change the operational, material, and structural conditions to adapt the model to new settings. Below is a summary of the software properties. In the descriptions, names of interfaces in the software use initial capital letters (such as Events or Parameters).

The software is embedded in COMSOL Multiphysics and has nodes corresponding to different properties in the model. On the top level, there are three components: 2D, 1D, and 1D Multi-ion. The most appropriate one for a given simulation can be run via the corresponding Study node. Each of these nodes has interfaces corresponding to the main behaviors (Fig. 1a). There is a Tertiary Current Distribution interface that calculates the currents and ionic transport. In 2D, the Brinkman Equations interface calculates the water flow. There are also interfaces for Events (switching between desalination and regeneration), the effective voltage in CC/CV mode (cell voltage and external voltage), Donnan/micropore potential (charge/adsorption balance), and flow mode. The Geometry interface makes it possible to change the device structure.

The interfaces provide the option to enable sub-interfaces for specific devices and operations. For instance, the Tertiary Current Distribution has a sub-interface that can be enabled for membranes and intercalation particles. FCDI can be enabled under the Adsorption sub-interface. The other interfaces have similar options, such as enabling CC/CV under the charging-mode interface. These interfaces contain the equations that the software solves numerically to produce the output (Fig. 1b).

The main part of the software to look at when setting up a simulation for a new device is the list of Parameters. The parameters are split into groups for clarity. The fitting parameters include the total circuit resistance (charging speed), the capacitance (storage capacity), and the micropore attraction (charge efficiency). There are also standard parameter lists for the structural, material, and operational conditions. Finally, optional parameters correspond to features that can be enabled.

The complexities of the CDI process have traditionally made it very difficult to make models that avoid crashing when the conditions become complicated. To address this, we incorporated stabilizing

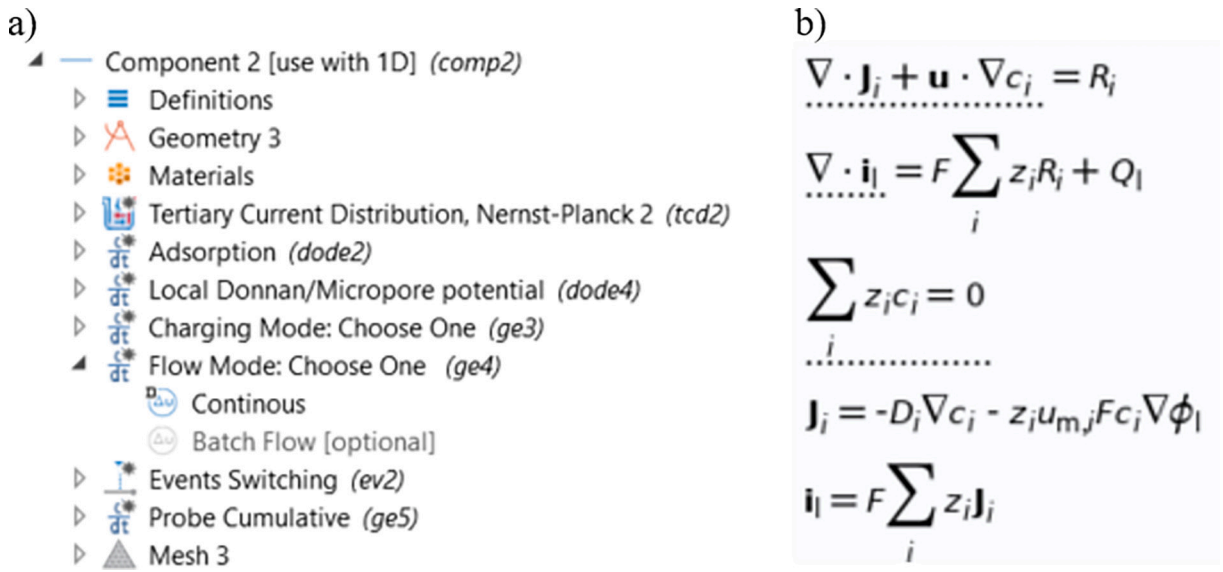

Fig. 1. (a) A screenshot of the interfaces in the 1D model. As shown in Flow Mode, the interfaces can be expanded so that sub-interfaces can be enabled to change the operation type. (b) Every interface shows the corresponding equations that the software solves. Here, the screenshot shows the ionic transport in the electrolyte.

measures inspired by control theory. Instead of requiring an exact adsorption balance in the single/multi-ion solution, the conditions are relaxed so that the ideal and momentaneous adsorption balances are calculated. These are then corrected with a K-controller.

3.3. Benchmarking

The developed software was tested for performance and compared with earlier works. The tests were performed on a computer with an Intel Core i5-9300HF (2.40GHZ) processor and 8.00 GB RAM. The performance was tested in two main categories. The first represents stable conditions (conditions from Ref. [21], CV charging at 0.6 V). That provides an estimate of the inherent performance and stability of the method. The second category represents unstable conditions. The most typical situation when instability emerges is when the device is ion starved, so this is chosen for the test. Ion starvation can be ramped up by testing successively higher voltages while keeping other conditions constant.

Newly developed software features have been tested as well, but due to the lack of earlier objects for comparisons they are reported in isolation. However, the stability of the new features can still be compared with the performance for the stable conditions above.

A complete list of model parameters, including their values, can be found in the default configuration of the deposited software. The software groups the parameters according to the types of simulations they are relevant to. The fitting parameters are relevant to all simulations. These are the parameters that should be derived from experiment data. Specifically, they correspond to the three main degrees of freedom: charge, charge efficiency, and charging rate. There are also parameter groups corresponding to the operation, the structure, and the materials & solution. Finally, there are internal parameters and parameters for numerical stabilization.

3.4. Tutorial

A longer tutorial video has been deposited and Mendeley Data (Nordstrand, Johan (2023), "SofTer Software and Tutorial ", Mendeley Data, V1, doi: 10.17632/twx7z52btv.1). The video shows how the use the software for the various types of simulation modes.

4. Results and discussion

Here, we will present the simulation performance with the new theory and software. The software can do lots of studies, and we have chosen to present four case studies. The first is the core case, showing classic CV charging as well as some other operational modes. These are also included in previous software [26], and the case study compares the effectiveness. This is important for understanding the general accuracy and stability of the new methods.

The rest of the cases correspond to newly developed features. The second case study is intercalation materials. These add complexity to the model formulation since the ions can diffuse into the particles at every position in the electrodes. Earlier studies have investigated some of these materials in CDI, but there has been no comprehensive integration with standard CDI methods. The third case study is multi-ion solutions. Time-dependent simulation of such conditions is challenging because of the adsorption balance between all ionic species, which makes traditional simulations unstable and unreliable. The fourth case study is flow-electrode CDI. Models exist that calculate FCDI performance in the steady state. However, time-dependent dynamics are more challenging since the model must describe the influx of new electrode material.

A prerequisite for having methods for these cases is that the corresponding theory has been derived. This can require a lot of effort but is reasonably straightforward since these physical situations are often well-known individually. A greater obstacle is numerical stability. That is, direct computational implementations will often fail even if the theory is physically sound. This is because the FEM programs cannot solve the posed equations with adequately small numerical errors. For this reason, a central part of the case studies will concern the numerical stability of each method.

4.1. The basic model

4.1.1. Case study: CV charging

The fundamental theory covers the common operations with ordinary CDI. Specifically, the default setting in the software corresponds to fb-CDI with carbon electrode in a continuous mode and CV operation. The results compared with experimental data are shown in Fig. 2. Notably, the difference in this macroscopic output is small when comparing the 1D and 2D models. So, fast computations in 1D can be sufficient for calculating the output performance, while 2D gives a better

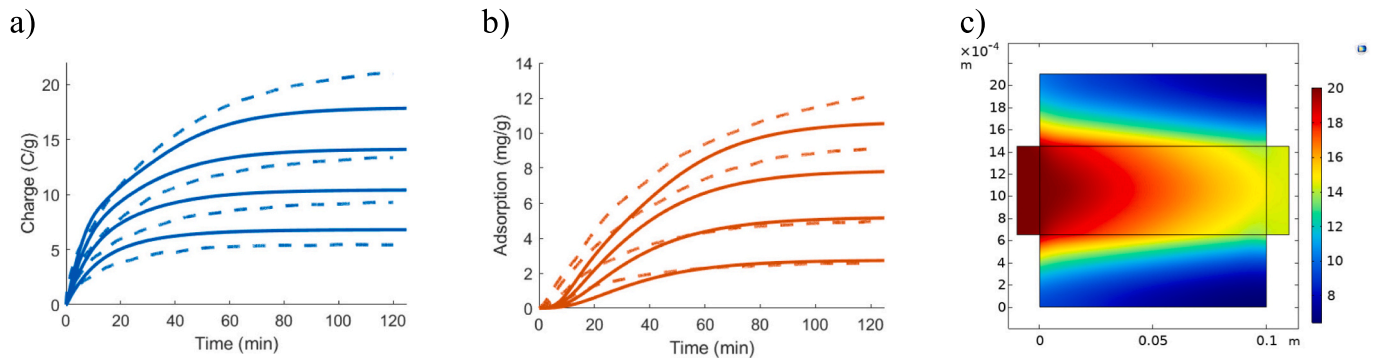

Fig. 2. Performance during charging of a CDI device with various CV voltages. The model lines have been calculated with the 1D model (a) The experiment (dashed lines) and model (full lines) cumulative specific charge. (b) The net removal from the output stream for the same model and experiment. (c) The internal concentration in the 2D model at the point of lowest effluent ion concentration with 0.6 V. The graphics are directly exported from COMSOL without postprocessing to show how the raw results can look.

description of the internal behavior of the device. Compared to earlier works with the mD model [21], the timescales of charge and adsorption are better here. Compared to earlier works with the ELC model [26], this work has a better description of the suppression in charge rate at the highest voltage (suggesting this model captures more detailed trends). Still, there is some deviation, which can mainly be attributed to differences in the equilibrium state caused by non-constant capacitance, as noted in previous works.

4.1.2. Numerical performance

As a benchmarking comparison, the 2D model with default settings takes 3 min 27 s to compute a full cycle on our laptop. The 1D model takes 26 s. Our earlier software in 2D computed in 22 s. The reason the software here is slower is that the tertiary current distribution requires more computational effort than the secondary current distribution that was used earlier. However, the speed is fast enough that the software is viable for research studies on normal computers. Clusters are not required.

Higher voltages tend to be less stable because the ion concentration becomes more depleted. In our old 2D software, the computation time rose from 22 s to 37 s at 1 V charging. Meanwhile, 1.2 V cannot be computed. Earlier works take much longer and are also limited to 1 V [21,22]. To be clear, this is a limit for the specific set of conditions and concentrations, not a limit for what the computations can handle in general. The new 2D model went up to 7 min 5 s, which is around twice the time of the stable conditions.

The new 1D model requires 26 s at 1 V, meaning the time is unaffected by low-degree starvation. At 1.6 V, it computes in 30 s. The upper limit is 2.2 V, which is computed at 30 s. Interestingly, the stability limit is sharper for the 1D mode, in the sense that the time is almost the same until it cannot compute at all. Another point to note is that the switching seems to be the limiting factor now, so even higher voltages can be computed if only the desalination phase is tested. Notably, the simulation does not include effects such as electrolysis or other Faradaic leakages that would occur at these voltages, so the voltage simulation is an idealized way of testing the starvation robustness.

Without stabilization, the 1D model cannot compute above 1.2 V. This goes to show that proper stabilization is essential for computing unstable conditions. We also tested other stabilization methods, such as introducing an artificial resistance that is inversely proportional to the concentration. However, these alternative methods were less stable. An advantage of the proposed method is also that it is clearer how much effect the stabilization has on the results since the lower concentration limit is raised from zero to a distinct small number.

Put together, we can say that the approach with the tertiary current distribution takes more time than some of the simpler models. At the same time, the 1D version was shown to be stable over a much wider range of conditions previously. Overall, we can say that the new software is sufficiently fast for laptop computations, although we recommend using 1D instead of 2D for unstable conditions.

4.1.3. Analysis

The case study results suggested that the simulation accuracy under stable conditions is limited by the theory rather than the FEM implementations. For instance, introducing a non-constant capacitance would raise the simulated accuracy, with everything else in the software being the same. That would suggest that the software could, in principle, be extended to include any new theory as long as there is stability. A conclusion, then, is that computational analyses ought to probe the numerically unstable regions of performance to better understand the process. These will be the performance regions that constrain what processes can be simulated.

The results confirm that computational time can be a proxy for stability. This can be seen in the voltage scan, wherein higher voltages raise computational times until the program crashes completely. Hence the relevance of analyzing computation times and stability together, since both indicate what theory is possible to implement with FEM.

The tests indicate that numerical instability comes when there are sharp changes with time. For instance, the process is less stable when the voltage jumps from 1 V to 0 V. Another problem is concentration shocks, as also noted in previous works. These reduce stability since there are sharp drops in concentration within the electrode between the region that has an ion and the region that is depleted. While similar results have been found in earlier studies, we here go further and find two instability points. Firstly, computations from the previous section that crash at around 1.2 V do so because the concentration reaches zero within the electrode at some point during the computation. Secondly, the calculations that crash above 2 V do so because ions cannot enter the electrode at the same rate as they are removed. In reality, the solution resistance would rise until there is balance, but this situation is computationally unstable.

The general principle for numerical instability is thus that they are connected to physical processes with rapid changes. The way the software handles this is by introducing artificial stabilization factors. For instance, the voltage is gradually raised from zero instead of jumping. An artificial resistance is added to slow the charging process when the electrodes are depleted. The balance of adsorption between ionic species is handled with a delay. Overall, these stabilizing measures should stop extreme conditions from spiraling out of control without affecting the simulation output. For instance, stopping the concentration from going below 0.001 mM during starvation is much more stable and marginally different in the output compared to having no lower limit.

4.1.4. Software variants

Continuing with the same device, it is also possible to simulate operations such as CC charging (Fig. 3ab), batch flow (Fig. 3c), pre-charged electrodes (Fig. 3d), membranes (Fig. 3e), and ft-CDI (Fig. 3f).

In general, we see that the CC charging has slower initial charging and more balanced removal with time, aiming at better energy efficiency. However, it can take a long time before the output stabilizes, which reduces the speed of the process (Fig. 3a). With the events interfaces, it is also possible to select upper and lower limits for the voltage instead of switching by time (Fig. 3b). Another way to raise the output speed is to use a flow-through setup instead of a flow-between setup (Fig. 3c). The ft-CDI typically improves output speed at the cost of extra energy from pumping, although the pumping energy is not directly reported in the software.

The batch flow means the influx concentration is lowered and then stabilizes as the electrodes become saturated (Fig. 3d). Notably, the concentration in the batch mode can be measured either at the inlet (i.e. the batch concentration) or the outlet (the device concentration). These reach the same values in the end, but measuring the effluent concentration gives a behavior that looks like a mix of the classic continuous and batch modes.

Pre-charged electrodes raise the charge efficiency since they shift the potential window relative to the PZC (Fig. 3e). Such pre-charge can be achieved, for instance, by fluorinating the electrodes to introduce charged groups [15]. Membranes raise the charge efficiency too (Fig. 3f). However, the mechanism is somewhat different. For low voltages (non-starved), the main difference is that co-ions are prevented from leaving, which raises charge efficiency. But, since the co-ions are kept in, the membranes also raise the ion concentration in the electrode pores. Normally, ion starvation can reduce the charging rate because the effective capacitance is much lower at low concentrations, meaning the device cannot charge maximally until the electrode is replenished to bring back the full capacitance. The membranes remove this problem, allowing the device to be much more effective at low ionic concentrations.

4.2. Intercalation materials

The basis for the simulation with IHC materials is that the particles form an extra dimension on the electrode. So, the same model setup as earlier can be used to calculate charging current and adsorption from the solution, which leads to corresponding charge and concentration at the surface of the particles. However, the ions at the surface of the particles can also diffuse deeper to allow new ions to reach the surface.

4.2.1. Case study: NiHCF

The intercalation model was tested against data in the literature, from Ref. [16] (Fig. 4). The particles in this case are Prussian blue analogs with nickel (NiHCF). The graphs show the relationship between the charging state and the voltage over the electrode. The voltage required to drive the equilibrium adsorption varies somewhat with the charging state, but mainly there is a rapid change in voltage if the particles approach a fully charged or depleted state. Overall, there is strong agreement between the simulation and the experiment data.

4.2.2. Numerical performance

The standard computation with the IHC took 42 s (using the initial 1D model with intercalation enabled). The computational stability of the simulation depends mostly on the charging state. Without stabilization, the model tends to crash when the state of charge reaches around 99.9 % or 0.1 %. This matters in CV charging because the model might crash instead of showing that the adsorption stops. CC charging with a high threshold can have similar issues. The model tends to compute with the stabilization added, although the results can sometimes be slower. The stabilized model took 1 min 8 s to compute with a CV voltage that was high enough to fully charge the IHC particles.

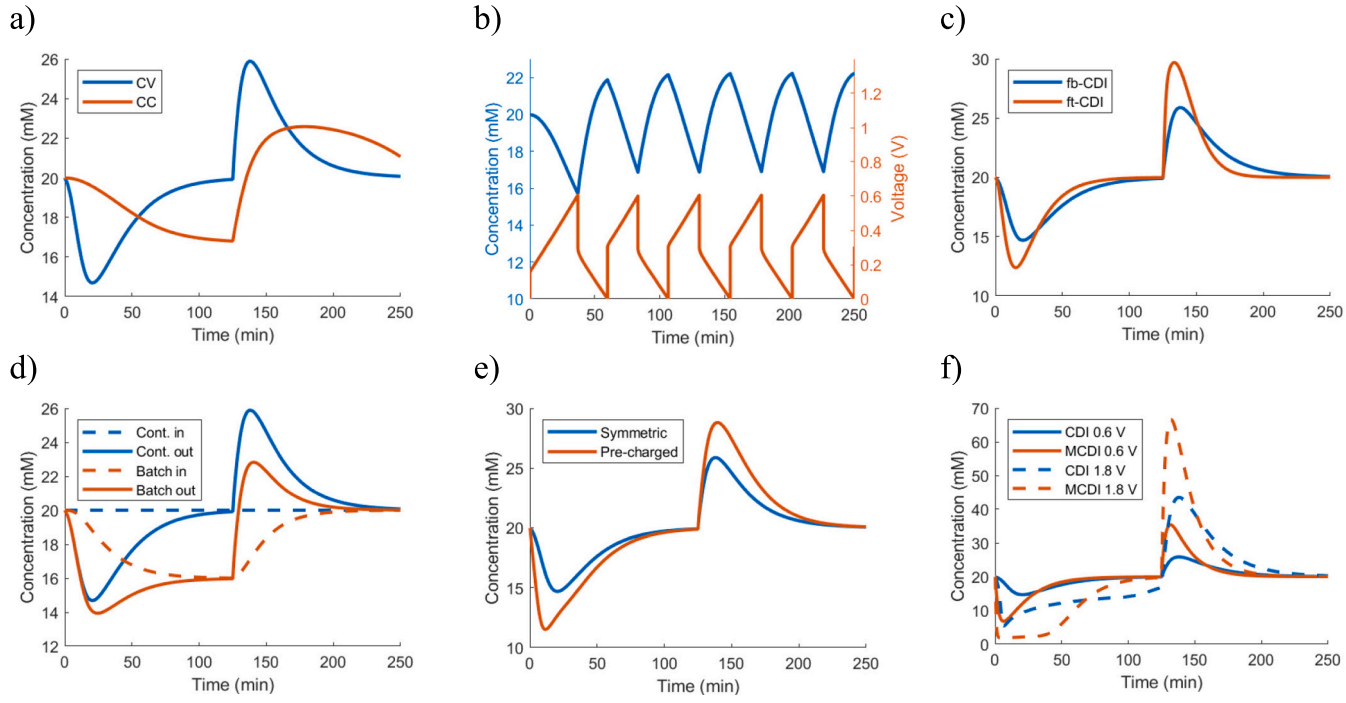

Fig. 3. Various operational modes in the CDI processes. The model is tuned with data from Ref. [21]. Unless otherwise noted, the voltage is 0.6 V. The voltage is low to represent stable conditions. (a) The effluent ion concentration is compared for CV and CC charging. The CC current is chosen such that the total charging is the same in the desalination phase. (b) Multiple cycles of CC operation using 0.6 V as a threshold for switching instead of a fixed time. The current is twice that in (a). The blue line corresponds to the concentration and the red line corresponds to the voltage. (c) A comparison between the continuous and batch flow. The effluent and the inlet (batch) concentrations are shown. (d) The same CV charging as in (a) is compared with pre-charged electrodes of 0.5 V, which raises the charge efficiency to nearly 100 %. (e) Comparison between CDI and MCDI for two voltages. (f) Comparison between the standard fb-CDI performance and the ft-CDI.

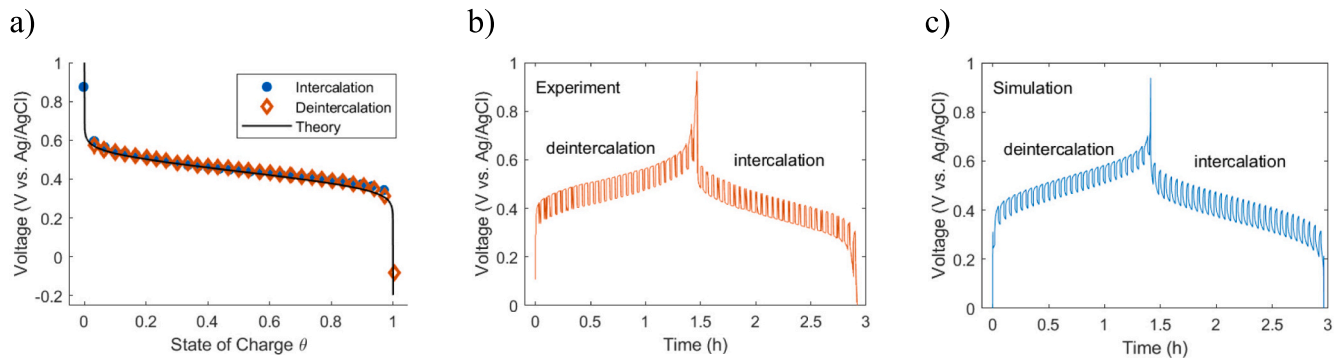

Fig. 4. Simulated and experimental behavior for a device with IHC. The experiment data was extracted from Ref. [16] while the simulations and graphics are new. (a) The connection between voltage and charging state in the IHC was compared to the theory in the Frumkin equation. (b) This is the experiment trend for time-dependent charging. The operation alternated between charging at 5C and resting periods at 0 A to ensure that the equilibrium charging state was approximately held throughout. (c) The simulated voltage profile for the same operation as the experiment and with the deduced materials parameters from the equilibrium graph in (a).

4.2.3. Analysis

Intercalation is an important case study since the theory adds a lot of complexity. There is both adsorption/desorption from the surface and internal transport. The results from the numerical study, however, suggest that the numerical complexity is not that much higher. The equivalent to depletion instability from the earlier section is here that the total charging degree is near 0 % or 100 %.

An insight we get from the case study is that the CDI process is reasonably decoupled. That is, features such as intercalation materials can be added without changing other parts of the FEM implementation. This is promising, as it indicates the possibility of constructing a universal CDI model.

4.2.4. Software variants

Intercalation in the software is implemented as an additional electrode interface. It could thus be enabled for either electrode, which is relevant to e.g. battery electrode CDI [16]. It can also be used separately or in conjunction with normal EDL adsorption. Enabling both would be relevant for systems that use intercalation particles grown on ACC, for instance [27]. However, it is worth noting that parameter fitting because more complex if there are many effects at the same time (both the intercalation and EDL capacitance need to be identified).

4.3. Multi-ion solutions

The multi-ion model has the same structure as the single-ion model, except more ions are added. The control system that previously balanced the charge efficiency now also balances the relative adsorption of each ionic species.

4.3.1. Case study: two monovalent cations

The multi-ion model was tested against our earlier data in the literature, from Ref. [26]. Here, the solution contains one anion and two cations. As normal, the circuit resistance and total capacitance can be determined from the total current (Fig. 5a). Having these, the remaining fitting parameters are the micropore attractions for each of the ions. Since we require that the electrodes are net uncharged, one of the attraction parameters can be calculated based on the other two. Thus, we fitted these parameters for the two cation species to get the proper charge efficiency for each of these.

There is good agreement between the theory and experiment (Fig. 5b), and it is substantially better than the previous work [26]. Interestingly, the simulated effluent Na^+ concentration captures the nuances in the charging phase (the experiment shows a net release in the middle of the phase). On the other hand, there is some deviation in accuracy for Cl^-.

4.3.2. Numerical performance

The computation took 24 s on the laptop for the 1D model. The raised computation time reflects the increased complexity of the model. The difference is marginal under normal conditions, although it tends to compound with other destabilizing effects, such as 2D calculations or starved conditions.

Fig. 5. The operation of an FCDI device. The experiment data are from Ref. [26] and the model lines are new. (a) This is the measured current, based on CV charging and discharging. (c) The measured effluent concentration from the device for each of the ionic species. The dots correspond to the experimental data and the lines are from the model.

4.3.3. Analysis

The numerical testing highlighted that a core challenge with multi-ion solutions is that the ionic species correspond to different charge efficiency (micropore attraction) on the electrodes. This means many combinations of parameter values give a similar numerical performance. On the other hand, the relative values of these parameters can also make a substantial difference in the qualitative behavior of the effluent concentration. This makes it harder to construct automatic schemes that find the globally best parameters.

Another conclusion from the simulations is that the flow mode and flow direction matter. In single-ion ft-CDI, since there is electroneutrality and Faradaic reactions are not considered, there is no difference in predicted performance depending on the flow direction. However, in the multi-ion solution, the charging state affects the adsorption balance even if there is net charge neutrality. The time-dependent relative removal (selectivity) of the process will thus depend on the flow direction. For instance, if the cathode is more selective towards Ca^{2+} than Na^{+}, then the initial relative removal of Ca^{2+} is higher if the cathode is downstream compared to upstream.

Overall, we can say that multi-ion solutions are one of the most difficult situations to simulate because of the issues with getting stable and consistent results. This suggests that more study is needed to better understand how well multi-ion behavior can be predicted under varying operations and device structures.

On the other hand, it is notable that the computational speed was reasonably fast despite the added complexity. Our testing showed that requiring the adsorption balance to be exact leads to strong numerical instability, whereas the relaxes approach presented here gives the same output performance at greater stability. This implementational approach is new compared to classic implementation schemes in CDI and could be a tractable approach in future research efforts that seek to develop theoretical results into computational methods.

4.3.4. Software variants

The software enables multi-ion solutions to be introduced in various CDI versions, such as intercalation and FCDI.

4.4. FCDI

The FCDI model is built on top of the ordinary model. That is, the difference between the FCDI model and the normal CDI model is that the FCDI model contains electrode replenishment. So, the charge on the electrode is determined by the charging rate and the influx of new electrode mass. Meanwhile, the control system for adsorption continues to adapt the adsorption of each ionic species to the charging state.

The FCDI simulation results have been tested against data in the literature, from Ref. [12]. During the operation, the current is gradually increased to test the performance at various charging rates. The model uses the same input current as in that work (Fig. 6a). For a fixed set of operating conditions, the voltage depends on the capacitance and circuit resistance (Fig. 6b). Under normal conditions of constant current, both have a linear effect on the steady-state voltage. However, the voltage rises faster when the current is high enough to cause starvation near the electrode surface, thus inducing substantial resistance in the solution. Finally, there is good agreement between the model and experiment for the effluent concentration (Fig. 6c). The error can mainly be attributed to uncertainty in the flowrate, which is a main determining parameter for how the input current translates to output concentration. Also, the experiment in Ref. [12] shows ideal charge efficiency (their Fig. 2). That is the case here by necessity since be approximated the membranes as fully blocking.

4.4.1. Numerical performance

The full computation took 18 s on the laptop (1D model). This is close to that in the other operations. As before, most of the time is consumed in initializing the model, so the difference in the operation type and length is marginal. Starvation raises computational times as usual. However, the situation here is mostly binary. The simulation crashes if the current is so high that the concentration near the electrode surface hits zero and the voltage diverges. But the speed remains fast even under starvation, to the extent that the testing conditions are physically possible to implement.

4.4.2. Analysis

A conclusion based on this testing is that the available concentration near the surface of the electrodes is limiting the speed of the operation. This could thus be raised with a higher flowrate or smaller dead volumes (spacers) in the FCDI cells. Micro-fluidics-based cell designs that improve mixing could also be beneficial since the ion starvation is typically localized at the electrode surface.

4.4.3. Software variants

FCDI is implemented as an added replenishment effect for the EDL electrodes. This means it can be combined with varying operations as normal.

4.5. Outlook

4.5.1. Limitations

The biggest limitation of the current software is that Faradaic reactions are not included. It can be included by just adding an interface in the software, so it is not difficult in principle. Rather, the limitation with the tertiary current distribution is that leakage current can only be added if the ionic species that participate in the leakages are also added. This makes the results somewhat more complicated to interpret, as opposed to earlier results with the secondary current distribution [28]. In other extreme cases, accuracy is limited by the precision of the theory. For instance, low ionic concentration can lead to high resistance. This is

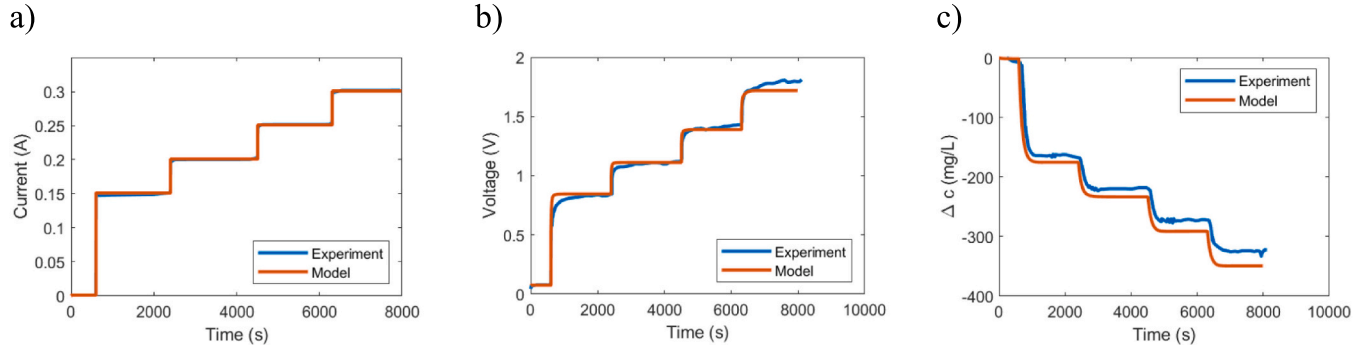

Fig. 6. The operation of an FCDI device. The experiment data are from Ref. [12] and the model lines are new. (a) The input current. (b) The measured external voltage. (c) The measured effluent concentration from the device. The y-axis shows the difference between the influent and effluent concentrations.

generally fine, but the method in the software for calculating resistance can always be exchanged for a more detailed method if necessary. However, the most common issue with specifically low concentrations is poor stability, which is one of the main things this work solves.

4.5.2. Flexibility

A highlight that is stressed in the work is flexibility. By flexibility, we mean that the same software can be applied to lots of different user cases with minor changes. So, the same basic theory works for many types of CDI architectures. This can be seen throughout the user cases. In the first (core) case, the different operations can be achieved by just turning on the corresponding interfaces. The intercalation materials are similarly a material effect that can be enabled on the base model. The multi-ion case has a separate set of interfaces that are ready to use. FCDI just requires that the interface for electrode replenishment is turned on. It should also be noted that all interfaces are implemented so that they fit any change in geometry automatically. The flexibility thus comes from the fact that specialized operations can be enabled as additions to an existing model with minimal changes.

Continuing the geometry discussion, the software enables simulations in different dimensions. Raising the dimensionality adds precision although the difference is marginal in simple use cases. More importantly, it makes it possible to evaluate asymmetric structures (see 3D discussion here [23]). Another value of the FEM methods is that they can be compared with idealized 0D models to see how much unideal mechanisms affect the end process (e.g. internal transport mechanisms). Thus, they can be great for discovering underlying reasons in cases where experiments do not agree with expectations of what should happen in a system (an example is our study on bipolar electrodes [29]).

Another point to note about flexibility is that material-based properties such as ion selectivity and charge efficiency are invariant of the CDI methods. So, the same software works for both ft. and fb-CDI, for instance. The output selectivity might not be the same, but the difference will be captured by the model since the material behavior and the transport are included. MCDI typically does not have the same charge efficiency as CDI, but membranes exist as an addition in the model. This means the same framework is generally applicable. One could also argue that adsorption on carbon particles in FCDI might not have the same behavior as carbon cloth in CDI. However, changes in material types are reflected in the fitting parameters, while the same model structure still holds.

Interestingly, the biggest obstacle to a unified model might be usability rather than theoretical accuracy. While the results suggest that a single software could implement most CDI variants, having a unified model also means that there are lots of interfaces to navigate for a person who is learning to use the software. It is thus an open question if it is more useful to continue to develop a unified model by making the implementation easier to navigate, or if it is ultimately better for the CDI community to have a larger set of smaller software that are specialized for different tasks. Probably, the best way forward is to develop a unified software in which the user chooses from the start what types of CDI methods to run, and the rest of the interfaces are hidden.

4.5.3. Role of simulations in practical applications

It is also worth discussing the role and impact that software like this can have on the practical application of CDI technologies. The software can aid in discovering operations and device structures that substantially improve performance. A concrete example is bipolar electrodes [29]. Given that the behavior of a single CDI cell is known, the software can predict what the performance will be in new device configurations. In the bipolar case, we could predict that a cell stack with all potential applied across the ends of the stack is faster than if all electrodes have separate connections. Specifically, it is faster proportionally to the stack size, meaning the potential payoff is huge. The common role the software can have in these discoveries is as a part of exploratory or focused investigations.

If we look for good output but do not know the desired operation/architecture, we could call that an exploratory investigation. For example, an experimental study could find that output selectivity is much lower experimentally than we might expect, so we look to improve the output. However, it is unclear what aspect of the operation/architecture is giving bad results. A typical software workflow could then be: 1. Implement the software under known conditions and verify with experiments. 2. Gradually make the operation more like the operation in the original experiment. In each step, look at the internal behavior of the CDI device to see where it deviates from the ideal expected behavior.

In this case, the role of the software is to provide a deeper understanding of the experimental system. By finding the important features and effects that were previously not considered, this understanding can become a basis for future experiments.

If the desired operation/architecture is known but the output is not, we could call that a focused investigation. For instance, we know that we want to construct a bipolar stack but we do not know how if works. As a principle, theoretical findings are more likely to be true if the same findings can be reached with different approaches. A way to use the software in a theoretical study would thus be to integrate it in three steps. 1. Consider what should happen in the investigated case based on general and well-known principles about CDI. 2. Construct a pen-and-paper model and calculate what should happen in the ideal case. 3. Use the software to investigate what happens in a realistic system and compare it with the idealized model.

In this case, the role of the theory and software is to propose new device architectures that could be implemented in practice.

5. Conclusions

In this work, we have presented theory, software, and a software tutorial for the multi-modeling of the CDI process. The result section demonstrated that numerical instability can be a limitation to what CDI process can be computed in a simulation. Simulation times were shown to get longer as computations gradually became less stable, meaning we could estimate the stability under varying conditions by looking at changes in computational times. Typically, a given operation becomes numerically unstable when there are rapid changes in the physical system.

To make it possible to simulate a wider range of CDI processes, we constructed a new simulation approach based on a tertiary current distribution. This approach treats each ionic species individually, meaning the simulation can be effective if stable. Because the fundamental approach is not directed towards a specific application, we could incorporate different applications as additions to a larger core framework. This makes the model more flexible. Also, the stability could be handled by introducing stabilizing factors inspired by control theory.

Finally, software has been constructed based on all the developments in the work. The software is openly available in the link under the “data availability” heading. Having such software speeds up and simplifies the simulation process compared to the situation where all researchers must build their own software from scratch for every new study. So, it could serve as an entry point and a tutorial, as well as facilitate a broad range of research studies that would otherwise not be conducted.

CRediT authorship contribution statement

The work was performed by a single author.

Declaration of competing interest

The authors declare that they have no known competing financial interests or personal relationships that could have appeared to influence the work reported in this paper.

Data availability

Nordstrand, Johan (2023), "SofTer Software and Tutorial ", Mendeley Data, V1, doi: 10.17632/twx7z52btv.1

Acknowledgments

J.N. would like to thank the Swedish Research Council (Diary No. 2018-05387) and J. Gustaf Richert Foundation (Diary No. 2020-00584) for funding the work. J.N. also acknowledges a great discussion with Prof. Matthias Franzreb that inspired some of the work in tertiary current distributions, including ideas on stabilizations.

References

[1] S. Porada, R. Zhao, A. Van Der Wal, V. Presser, P.M. Biesheuvel, Review on the science and technology of water desalination by capacitive deionization, Prog. Mater. Sci. 58 (2013) 1388–1442, https://doi.org/10.1016/j.pmatsci.2013.03.005.
[2] M.E. Suss, S. Porada, X. Sun, P.M. Biesheuvel, J. Yoon, V. Presser, Water desalination via capacitive deionization: what is it and what can we expect from it? Energy Environ. Sci. 8 (2015) 2296–2319, https://doi.org/10.1039/C5EE00519A.
[3] M.A. Anderson, A.L. Cudero, J. Palma, Capacitive deionization as an electrochemical means of saving energy and delivering clean water. Comparison to present desalination practices: will it compete? Electrochim. Acta 55 (2010) 3845–3856, https://doi.org/10.1016/j.electacta.2010.02.012.
[4] T. Yu, H. Shiu, M. Lee, P. Chiueh, C. Hou, Life cycle assessment of environmental impacts and energy demand for capacitive deionization technology, Desalination 399 (2016) 53–60, https://doi.org/10.1016/j.desal.2016.08.007.
[5] K. Singh, G. Li, J. Lee, H. Zuilhof, B.L. Mehdi, R.L. Zornitta, L.C.P.M. de Smet, Divalent ion selectivity in capacitive deionization with vanadium hexacyanoferrate: experiments and quantum-chemical computations, Adv. Funct. Mater. 31 (2021), https://doi.org/10.1002/adfm.202105203.
[6] L. Gan, Y. Wu, H. Song, S. Zhang, C. Lu, S. Yang, Z. Wang, B. Jiang, C. Wang, A. Li, Selective removal of nitrate ion using a novel activated carbon composite carbon electrode in capacitive deionization, Sep. Purif. Technol. 212 (2019) 728–736, https://doi.org/10.1016/J.SEPPUR.2018.11.081.
[7] L. Wang, S. Lin, Mechanism of selective ion removal in membrane capacitive deionization for water softening, Environ. Sci. Technol. 53 (2019) 5797–5804, https://doi.org/10.1021/acs.est.9b00655.
[8] C. Tan, C. He, W. Tang, P. Kovalsky, J. Fletcher, T.D. Waite, Integration of photovoltaic energy supply with membrane capacitive deionization (MCDI) for salt removal from brackish waters, Water Res. 147 (2018) 276–286, https://doi.org/10.1016/j.watres.2018.09.056.
[9] J. Nordstrand, K. Laxman, M.T.Z. Myint, J. Dutta, An easy-to-use tool for modeling the dynamics of capacitive deionization, J. Phys. Chem. A 123 (2019) 6628–6634, https://doi.org/10.1021/acs.jpca.9b05503.
[10] A. Thamilselvan, A.S. Nesaraj, M. Noel, Review on carbon-based electrode materials for application in capacitive deionization process, Int. J. Environ. Sci. Technol. 13 (2016) 2961–2976, https://doi.org/10.1007/s13762-016-1061-9.
[11] M. Qin, W. Ren, R. Jiang, Q. Li, X. Yao, S. Wang, Y. You, L. Mai, Highly crystallized Prussian blue with enhanced kinetics for highly efficient sodium storage, ACS Appl. Mater. Interfaces 13 (2021) 3999–4007, https://doi.org/10.1021/acsami.0c20067.
[12] C. He, B. Lian, J. Ma, C. Zhang, Y. Wang, H. Mo, T.D. Waite, Scale-up and modelling of flow-electrode CDI using tubular electrodes, Water Res. 203 (2021), 117498, https://doi.org/10.1016/j.watres.2021.117498.
[13] L. Wang, S. Lin, Membrane capacitive deionization with constant current vs constant voltage charging: which is better? Environ. Sci. Technol. 52 (2018) 4051–4060, https://doi.org/10.1021/acs.est.7b06064.
[14] W. Tang, J. Liang, D. He, J. Gong, L. Tang, Z. Liu, D. Wang, G. Zeng, Various cell architectures of capacitive deionization: recent advances and future trends, Water Res. 150 (2019) 225–251, https://doi.org/10.1016/j.watres.2018.11.064.
[15] E. Toledo-Carrillo, X. Zhang, K. Laxman, J. Dutta, Asymmetric electrode capacitive deionization for energy efficient desalination, Electrochim. Acta 358 (2020), 136939, https://doi.org/10.1016/j.electacta.2020.136939.
[16] S. Porada, A. Shrivastava, P. Bukowska, P.M. Biesheuvel, K.C. Smith, Nickel hexacyanoferrate electrodes for continuous cation intercalation desalination of brackish water, Electrochim. Acta 255 (2017) 369–378, https://doi.org/10.1016/j.electacta.2017.09.137.
[17] K. Singh, Z. Qian, P.M. Biesheuvel, H. Zuilhof, S. Porada, L.C.P.M. de Smet, Nickel hexacyanoferrate electrodes for high mono/divalent ion-selectivity in capacitive deionization, Desalination. 481 (2020), 114346, https://doi.org/10.1016/J.DESAL.2020.114346.
[18] P. Nativ, Y. Badash, Y. Gendel, New insights into the mechanism of flow-electrode capacitive deionization, Electrochem. Commun. 76 (2017) 24–28, https://doi.org/10.1016/j.elecom.2017.01.008.
[19] J. Nordstrand, J. Dutta, Simplified prediction of ion removal in capacitive deionization of multi-ion solutions, Langmuir 36 (2020) 1338–1344, https://doi.org/10.1021/acs.langmuir.9b03571.
[20] J. Nordstrand, J. Dutta, ELC: Software and Tutorial for Finite-element Modeling of Electrochemical Desalination, Under Rev., SoftwareX, 2022.
[21] A. Hemmatifar, M. Stadermann, J.G. Santiago, Two-dimensional porous electrode model for capacitive deionization, J. Phys. Chem. C 119 (2015) 24681–24694, https://doi.org/10.1021/acs.jpcc.5b05847.
[22] J. Nordstrand, J. Dutta, A new automated model brings stability to finite-element simulations of capacitive deionization, Nano Sel. 3 (2022) 1021–1035, https://doi.org/10.1002/nano.202100270.
[23] J. Nordstrand, L. Zuili, J. Dutta, Fully 3D modeling of electrochemical deionization, ACS Omega 8 (2023) 2607–2617, https://doi.org/10.1021/acsomega.2c07133.
[24] K. West, T. Jacobsen, S. Atlung, Modeling of porous insertion electrodes with liquid electrolyte, J. Electrochem. Soc. 129 (1982) 1480–1485, https://doi.org/10.1149/1.2124188.
[25] A. Rohatgi, WebPlotDigitizer, Https://Automeris.Io/WebPlotDigitizer, http://arohatgi.info/WebPlotDigitizer%0D, 2019. (Accessed 30 November 2021).
[26] J. Nordstrand, L. Zuili, E.A. Toledo-Carrillo, J. Dutta, Predicting capacitive deionization processes using an electrolytic-capacitor (ELC) model: 2D dynamics, leakages, and multi-ion solutions, Desalination. 525 (2022), 115493, https://doi.org/10.1016/j.desal.2021.115493.
[27] X. Zhang, J. Dutta, X-Fe (X = Mn, Co, Cu) Prussian blue analogue-modified carbon cloth electrodes for capacitive deionization, ACS Appl. Energy Mater. 4 (2021) 8275–8284, https://doi.org/10.1021/acsaem.1c01501.
[28] J. Nordstrand, J. Dutta, ELC : software and tutorial for finite-element modeling of electrochemical desalination, SoftwareX. 20 (2022), 101234, https://doi.org/10.1016/j.softx.2022.101234.
[29] J. Nordstrand, J. Dutta, Theory of bipolar connections in capacitive deionization and principles of structural design, Electrochim. Acta 430 (2022), 141066, https://doi.org/10.1016/j.electacta.2022.141066.